Modelling Simul. Mater. Sci. Eng. **19** (2011) 054003 (20pp) doi:10.1088/0965-0393/19/5/054003

Twisted and coiled ultralong multilayer graphene ribbons

Steven Cranford[1,2] **and Markus J Buehler**[1,2]

[1] Center for Materials Science and Engineering, Massachusetts Institute of Technology, 77 Massachusetts Ave. Room 1-235A&B, Cambridge, MA, USA
[2] Laboratory for Atomistic and Molecular Mechanics, Department of Civil and Environmental Engineering, Massachusetts Institute of Technology, 77 Massachusetts Ave. Room 1-235A&B, Cambridge, MA, USA

E-mail: mbuehler@MIT.EDU

Received 8 February 2011, in final form 29 April 2011
Published 23 June 2011
Online at stacks.iop.org/MSMSE/19/054003

Abstract

The mechanical behavior and properties of multilayer graphene sheets and nanoribbons have been a subject of intensive research in recent years, due to their potential in electronic, structural and thermal applications. Calculations of effective properties range from molecular dynamic simulations to use of structural mechanical continuum models. Here, structural and elastic parameters are obtained via full atomistic simulations, and a two-dimensional mesoscopic model for a sheet of graphene is developed utilizing coarse-grain bead-spring elements with rotational-spring potentials. The assertion of energy conservation between atomistic and mesoscale models through elastic strain energy is enforced to arrive at model parameters, incorporating normal and shear strains, out-of-plane bending and intramolecular interactions. We then apply our mesoscopic model to investigate the structure and conformational behavior of twisted ultralong multilayer graphene ribbons with lengths of hundreds of nanometers, representing several millions of individual atoms, beyond the accessible regime of full atomistic molecular dynamics. We find a distinct transition from a twisted (saddle-like) configuration to a helical (coil-like) configuration as a function of imposed rotation and number of graphene layers. Further, for single layer graphene ribbons, multiple, stable configurations occur at discrete rotations due to the surface adhesion. The model developed and applied here can be more generally used to investigate properties of other two-dimensional membrane and ribbon-like systems for mesoscale hierarchical material design.

(Some figures in this article are in colour only in the electronic version)

1. Introduction

Graphene sheets are one-atom-thick two-dimensional layers of sp^2-bonded carbon that have remarkable mechanical, thermal and electrical properties [1–3]. Experimental results establish graphene as one of the strongest materials ever tested in terms of elastic stiffness and ultimate tensile strength [3, 4]. The superlative properties of mono- and mulitlayer graphene sheets can facilitate the design of advanced composites with superior mechanical and electrical performance [5] and impel applications in novel nanostructures. The advantages of graphene-based material systems lie in the relatively flat, monoatomic sheet geometry that balances a high surface area with the mechanical strength of in-plane carbon bonding, with promising properties for energy storage [6, 7] and stretchable, more ductile microelectronics [8]. The desire to enhance the accessible atomistic surfaces and edges inherently limits the scale of such systems to the order of micrometers. However, even at this length-scale, bottom-up mechanical investigations are hindered by the computational expense of full atomistic representations, and conventional continuum theories cannot be applied to describe their structural and mechanical properties from the bottom-up. This calls for novel approaches to develop models to enable the engineering design of graphene materials.

A multitude of experimental approaches—including mechanical cleavage [9], top-down lithography and cutting [10], or peeling [11], as examples—are now applied to fabricate graphene sheets with desired shape and size. In particular, graphene nanoribbons—graphene sheets with large aspect ratios of length to width—present intriguing electronic properties due to their characteristic size and edge shape. Previous atomic-scale microscopy and spectroscopy studies revealed a significant variety of graphene conformations, where ripples, kinks and folds have been observed [12–14], depending on the geometry of graphene sheets and ribbons. These characteristic 'secondary structures' of graphene have prominent effects on the resulting functional material properties and have thus received considerable attention at the molecular scale [15–17]. However, application in electronic devices, nanoscale materials, etc, necessitates characterization at larger length-scales. This consequently results in a modelling impasse—the effect of such secondary structures, or hierarchical configurations, must be represented, but is limited by the length-scales accessible to full atomistic simulations. To fully utilize the design potential of graphene ribbons, hierarchical multiscale analytical methods must be developed that accurately describe the behavior of graphene ribbons at both the nano- and micro-scales.

Intermolecular interactions between graphene sheets require the development of coarse-grain techniques beyond the capacity of traditional continuum and structural mechanics. Previous multiscale modeling attempts have successfully implemented finite element representation of graphene via elastic plate formulations [18]—however, such elements neglect the adhesion and interactions critical to configurations of graphene structures, and were limited to monolayer graphene. Here, a method to bridge these two approaches is implemented, using concepts of hierarchical multiscale modeling. Mesoscale coarse-grain modeling does not intend to disassociate atomistic behavior, but rather incorporate multi-body atomistic interactions and properties into the intrinsic performance of coarse-grain potentials. Equivalent atomistic to continuum or structural mechanics approaches have been applied previously to both graphene sheets and carbon nanotubes, including truss-type analytical models [19], finite element beams [20] and uniaxial links with nonlinear rotational springs [21], as examples. Such techniques utilize equivalent elastic strain energy to simplify complex atomistic behavior. However, the components of such models are ultimately limited to atomistic scales, parametrically defining carbon–carbon bonding with equivalent elasticity models. The intent of a mesoscale model is to expand the atomistic to structural mechanics

approach to vastly larger systems. The parameters in the mesoscopic model are fit to reproduce elastic and adhesion properties of graphene sheets, thereby enabling the modeling of the dynamics of graphene sheets approaching the microscale over time-scales on the order of microseconds, bridging the length- and time-scale limitations of full atomistic simulations.

The focal point of this paper is the multi-scale development of a two-dimensional coarse-grain mesoscopic model that can replicate the mechanical behavior of mono- and multilevel graphene in complex hierarchical configurations. Such methods are intended to simplify the simulation of more complex systems, such as composite polymer nanofilms [22, 23] or biological membranes [24] that require time- and length-scales beyond the reach of traditional molecular dynamics. With the developed mesoscale model, the structure and stability of twisted graphene nanoribbons are investigated.

2. Methods

A 'fine-trains-coarse' approach is implemented to produce mesoscale model derived solely from atomistic calculations. A series of full atomistic calculations of mechanical test cases (test suite) is implemented via classical molecular dynamics (MD) to derive a simplified set of parameters to describe the graphene sheet behavior. Similar modelling approaches have been used for the mesoscopic simulation of carbon nanotube bundles and arrays [25–28] for collagen systems [29, 30], for example. Here, we extend the concept to a two-dimensional representation. The model described hereafter has been previously implemented to investigate the stable folding of graphene sheets [31].

2.1. Full atomistic simulations and mechanical characterization

The test suite implemented to determine the parameters required for the coarse-grain graphene sheet consist of the following four loading cases: (i) uniaxial tensile loading to determine Young's modulus, E; (ii) simple shear loading to determine shear modulus, G; (iii) out-of-plane bending to determine the bending stiffness per unit width, D and (iv) a stacked assembly of two sheets to determine the adhesion energy per unit area, γ_L. The test suite was applied using a 100 Å $\times$ 100 Å graphene sheet with armchair orientation along the x-axis (zigzag orientation along the y-axis), as depicted in figure 1. The full atomistic investigations utilize the ReaxFF potential for carbon–carbon interactions [32, 33]. The first-principles-based ReaxFF force field has been shown to provide an accurate account of the chemical and mechanical behavior of hydrocarbons, graphite, diamond, carbon nanotubes and other carbon nanostructures [34–36] while it is capable of treating thousands of atoms with near quantum-chemical accuracy. A time increment is chosen to be on the order of femtoseconds (1.0×10^{-15} s). All full atomistic simulations are subject to a microcanonical (*NVE*) ensemble, carried out at a low temperature of 10 K to prevent large thermal vibrations. Temperature control was achieved using a Berendsen thermostat [37]. The MD simulations are performed using the massively parallelized modeling code LAMMPS [38] (http://lammps.sandia.gov/) capable of running on large computing clusters.

It is well established that the strain energy and deformation of graphene sheets can be described by continuum elasticity theory [39–44]. For the current model development, it is assumed that under small deformation, graphene can be approximated as a linear elastic isotropic material. Further, to take advantage of the two-dimensional planar arrangement, a plane stress approximation is utilized to calculate elastic strain energy implemented for energy conservation between atomistic and mesoscopic models. More complex elasticity models can be implemented to account for out-of-plane behavior, anisotropic and finite strain effects, but

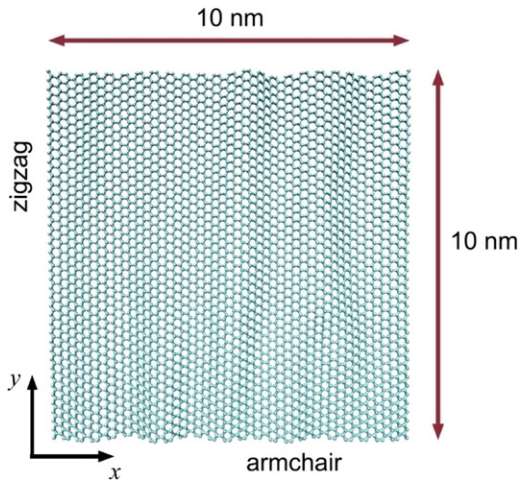

Figure 1. Full atomistic model of monolayer graphene sheet (100 Å × 100 Å) implemented in the first principles ReaxFF force field. Starting configuration for mechanical test suite required for coarse-grain model parametrization. Representative snapshot after equilibration at 300 K with small in-plane rippling due to thermal fluctuations. Armchair edges in the x-direction, zigzag edges in the y-direction. Formulated coarse-grain model for graphene ribbons considers mechanical parameters with armchair edges.

would require a more thorough suite of atomistic simulations to derive all pertinent parameters, and is beyond the scope of the current investigation. For plane stress, we define the stress–strain relationship as

$$\begin{bmatrix} \sigma_x \\ \sigma_y \\ \tau_{xy} \end{bmatrix} = \frac{E}{1-\upsilon_p^2} \begin{bmatrix} 1 & \upsilon_p & 0 \\ \upsilon_p & 1 & 0 \\ 0 & 0 & 1/2(1-\upsilon_p) \end{bmatrix} \begin{bmatrix} \varepsilon_x \\ \varepsilon_y \\ \gamma_{xy} \end{bmatrix}. \tag{1}$$

We define the strain energy as

$$U(\sigma, \varepsilon) = \frac{1}{2} \int_\Omega [\sigma][\varepsilon] \, \mathrm{d}\Omega, \tag{2}$$

where Ω is the representative volume under stress (here taken as the graphene sheet). The intent is to assert equivalence between elastic strain energy and coarse-grain molecular potentials.

Uniaxial tension and simple shear. A uniaxial tensile test was applied to the graphene sheet by implementing periodic boundary conditions along the x-axis only, and deforming the unit cell by stretching along the x-direction at a uniform rate (thereby inducing a uniform strain rate). To load the graphene sheet in pure shear, the bottom of sheet was fixed along the x-axis, while the top was sheared with a constant stretching along the x-direction at a uniform rate (inducing a uniform shear strain rate). In both cases, the strain rate applied was $1.0 \times 10^{-6}\ \mathrm{s}^{-1}$. See figures 2($a$) and ($b$). The virial stress is commonly used to relate to the macroscopic (continuum) stress in molecular dynamics computations. The components of the macroscopic stress tensor, σ_{ij}, in a volume Ω is taken to be [45, 46]

$$S_{ij} = \frac{1}{\Omega} \sum_{a \in \Omega} \left[-m^{(a)} v_i^{(a)} v_j^{(a)} + \frac{1}{2} \sum_{b \in \Omega} ((r_i^{(a)} - r_i^{(b)}) F_j^{(ab)}) \right], \tag{3}$$

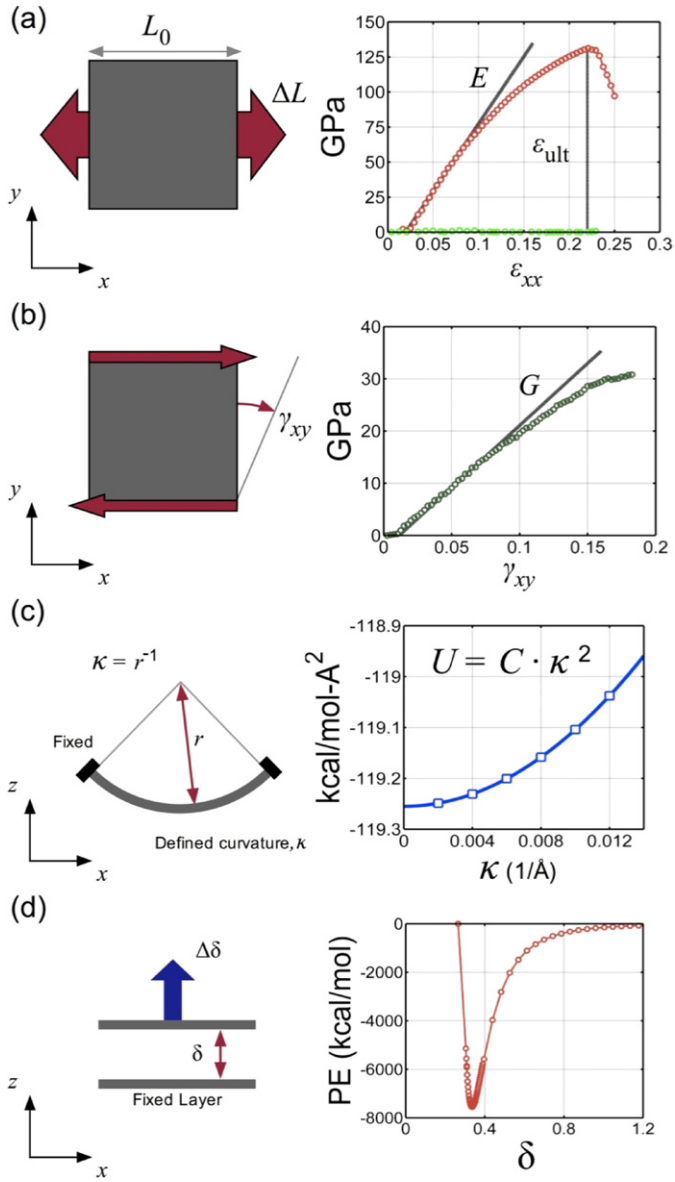

Figure 2. Applied mechanical test suite and summary of results. (*a*) Uniaxial tension test along the x-direction (armchair); plot of σ_{xx} versus ε_{xx}; linear fit to small strain to derive Young's modulus, $E \approx 0.97$ TPa. Also, we illustrate a plot of σ_{yy} versus ε_{xx} for which $\sigma_{yy} \approx 0$, supporting the assumption used for equation (6). Ultimate strain taken at point of maximum stress, where $\varepsilon_{ult} \cong 0.23$. (*b*) Simple shear test with plot of σ_{xy} versus γ_{xy}; linear fit to small strain to derive shear modulus, $G \approx 0.22$ TPa. (*c*) Bending modulus per unit length, D, determined via strain energy. The minimized potential energy per unit area is fitted by a parabolic function for a set of defined curvatures, κ. The bending stiffness is then determined from the constant as per equation (7). The plot given depicts the results for bilayer graphene. (*d*) Adhesion energy determined by a simple test in which the potential energy is plotted versus sheet separation. The energy minimum occurs at the equilibirum spacing ($D_{vdW} = 3.35$ Å), while adhesion strength is derived from the magnitude of the energy well. A summary of all results is given in table 1.

which generates the six components of the symmetric stress-volume tensor, S_{ij}, where $m^{(a)}$ is the mass of particle 'a', $v_i^{(a)}$ and $v_j^{(a)}$ are the velocities in the ith and jth vector component basis, $r_i^{(a)} - r_i^{(b)}$ denotes the distance between particle 'a' and atom 'b' along the ith vector component, while $F_j^{(ab)}$ is the force on particle 'a' exerted by particle 'b' along the jth vector component, and Ω is the volume. To reduce random and temperature-related stress fluctuations, in addition to averaging over the representative volume, Ω, the stress is averaged further over a small time interval of 100 fs around the desired time of the stress. The total stress can be calculated as

$$\sigma_{ij} = S_{ij}\Omega^{-1}, \tag{4}$$

where Ω is taken as the dimensions of the graphene sheet with a thickness equal to the van der Waals equilibrium spacing ($D_{\mathrm{vdW}} = 3.35$ Å). The graphene sheet was strained to 25%, which was chosen to encompass the deformation until fracture. The resulting stress–strain relationships can then be plotted (figure 2(*a*)). From equation (1), it can be shown that

$$\varepsilon_x = \frac{1}{E}[\sigma_x - \upsilon_{\mathrm{p}}\sigma_y] \tag{5a}$$

and

$$\gamma_{xy} = \frac{2(1+\upsilon_{\mathrm{p}})}{E}\tau_{xy} = \frac{1}{G}\tau_{xy}, \tag{5b}$$

where E is the desired Young's modulus and G is the shear modulus. From the results of the full atomistic simulations, for uniaxial strain, $\sigma_x \gg \sigma_y$ (figure 2(*a*)) thus we arrive at two simple linear elastic relations:

$$\sigma_x = E\varepsilon_x \rightarrow E = \frac{\partial\sigma_x}{\partial\varepsilon_x} \cong \frac{\Delta\sigma_x}{\Delta\varepsilon_x}, \tag{6a}$$

$$\tau_{xy} = G\gamma_{xy} \rightarrow G = \frac{\partial\tau_{xy}}{\partial\gamma_{xy}} \cong \frac{\Delta\tau_{xy}}{\Delta\gamma_{xy}}, \tag{6b}$$

The simulation returns a Young's modulus value of approximately 0.968 TPa along the armchair orientation (uniaxial strain along the x-axis) and 0.957 TPa along the zigzag orientation (uniaxial strain along the y-axis). We obtain a value of 0.224 GPa for the shear modulus. The results show good agreement with previous investigations where the determined Young's modulus of a single layer graphene sheet is reported on the order of ∼1 TPa, and a shear modulus ranging from 0.21 to 0.23 TPa, with negligible difference between armchair and zigzag orientations [19, 47–50].

The ambiguity for the thickness of graphene and carbon nanotubes has been discussed in a previous study [51] which suggested the stress and elastic moduli of monolayer graphene be reported in force per unit length (N m^{-1}) rather than force per unit area (N m^{-2} or Pa). Our value of the graphene in force per unit length is given by 289 N m^{-1}, which is close to the results reported in other works [44, 49, 52] (which are broadly in the range 235–354 N m^{-1} depending on the method used). Here, the label of 'Young's modulus' is only intended as a placeholder for the tensile behavior of graphene to parametrize a coarse-grain model—consistent definitions of cross-section thickness are maintained at both the atomistic and mesoscales, thereby negating any ambiguity of chosen thickness. In agreement with previous investigations, we assert that the continuum interpretation of Young's modulus, E, is not reflective of monolayer graphene, and is merely used here as a convenient convention for model development. Further, the introduction of multilayer graphene systems introduces finite thickness, allowing consistency in model parametrization. Through the use of common terms, more apt comparisons can be made with previous (and future) coarse-grain studies with other material systems [25, 31].

Regarding the attained value, recent study suggests that internal lattice relaxation, which effectively decreases the tensile stiffness of monolayer graphene, is not sufficiently reflected in common molecular potentials [44]. Thus, the axial stiffness (in-plane Young's modulus) has been reported in a range from approximately 0.7 to 1.03 TPa (assuming a thickness of 0.335 nm) [44]. To maintain consistency within our applied 'test suite', we use our determined value of 0.968 TPa for modeling, in agreement with reported experimental results [3]. Furthermore, the current investigation involves a structural comparison of twisted graphene nanoribbons, wherein variations in stiffness would only marginally affect results. Future refinements in the atomistic determination of elastic parameters could easily be implemented in the developed coarse-grain model.

The ultimate strain under tension was taken as the strain level at maximum stress ($\varepsilon_{\text{ult}} = 0.23$ at 131 GPa). It is noted that the ultimate strain does not necessarily represent the complete fracture of the graphene sheet, but merely local rupture and subsequent drop in load capacity. These values are in agreement with previous computational and experimental studies [3, 49, 50, 52].

Out-of-plane bending modulus. Due to the relative flexibility and single atom thickness of monolayer graphene, a mechanical bending test is difficult to implement [49, 51]. The isotropic bending modulus is determined by one-dimensional pure bending experiments using molecular statics, similar to previous coarse-grain [31] and full atomistic [11, 43, 53] investigations. To calculate the bending modulus of N layers of graphene, a rectangular sheet of the N layers was bent into a section of a cylinder with constant radius of curvature throughout the basal plane. The neutral plane for pure bending is parallel to the N layers and passes through the centroid of the bending cross section. The edges of the bent sheet were kept fixed and the bulk of the sheet was allowed to relax to an energy minimum. Energy minimization of the system was performed using a conjugate-gradient algorithm with an energy-convergence criterion implemented in the LAMMPS code. The bending modulus was calculated by fitting the energy-curvature data to the following expression [54]:

$$U_{\text{bend}} = \tfrac{1}{2} D\kappa^2, \tag{7}$$

where U_{bend} is the system strain energy per unit basal plane area, D is the bending modulus per unit width and κ is the prescribed beam curvature. Curvatures of 0.002–0.012 Å^{-1} (cylindrical radii of approximately 83 Å to 500 Å) were imposed on 1-, 2-, 4- and 8-layer graphene systems and the minimized energies plotted versus κ (representative results for 2-layer system given in figure 2(*c*)). The resulting bending stiffnesses were 2.1, 130, 1199 and 13 523 eV for 1-, 2-, 4- and 8-layer graphene, respectively [11]. Previous investigations report smaller values of monolayer bending stiffness, ranging from 0.69 to 1.5 eV [43, 48, 49, 53], dependent on technique (*ab initio*, MD, etc) and the chosen potential. As the current investigation compares multilayer structures—which are orders of magnitude stiffer than monolayer graphene—the determined value is deemed adequate. Thus, to maintain consistency within our applied 'test suite', we use the value of 2.1 eV for the modeling of single layer graphene.

Adhesion. We next characterize weak interactions (i.e. van der Waals interactions) between two graphene surfaces. For adhesion simulations, two copied graphene sheets are simulated together, moved into close proximity to one another, and then separated, with an energy minimization procedure undertaken at discrete distances. The geometric configuration at contact (energy minima) can be used to determine equilibrium distances, while the differences in energy minima between simulations at the equilibrium distance and at a semi-infinite separation can be used to extract potential energy gain of adhesion per unit area (figure 2(*d*)).

Table 1. Summary of results from full atomistic simulations.

Parameter	Value	Units
Young's modulus, E	968	GPa
Ultimate tensile strain, ε_{ult}	0.23	%
Shear modulus, G	224	GPa
Bending modulus, D		
1 Layer	2.1	eV
2 Layer	130	eV
4 Layer	1199	eV
8 Layer	13 523	eV
Surface energy, γ_{L}	260	mJ m^{-2}
Equilibrium spacing, D_{vdW}	3.35	Å

We find an equilibrium distance, D_{vdW}, of 3.35 Å, with a surface energy, γ_{L}, of approximately 260 mJ m^{-2}, which is in reasonable agreement with previous investigations (151 mJ m^{-2} [55] to 345 mJ m^{-2} [56]) and the current molecular model employed. Table 1 summarizes the results of all atomistic simulations.

2.2. Mesoscale model

We aim to arrive at a two-dimensional mesoscale model developed directly from the results of atomistic simulations. The basis of the mesoscale model is represented by a function of the total energy of the system expressed as

$$\phi_{\text{system}} = \phi_{\text{T}} + \phi_{\varphi} + \phi_{\theta} + \phi_{\text{adhesion}}, \tag{8}$$

where ϕ_{T} is the strain energy due to axial stretching, ϕ_{φ} is the energy due to shear deformation, ϕ_{θ} is the energy due to out-of-plane bending and ϕ_{adhesion} is the energy due to inter-sheet adhesion (weak interactions). The total energy contribution of each is calculated by a sum over all defined bonded (distance), triple (angular) and pair-wise (distance) interactions in the system (figure 3(*a*)). A similar approach is used in the development of bead-spring mesoscale models of carbon nanotubes [25, 27, 28]. To associate full atomistic results with mesoscale model parameters, we implement an equivalent energy approach.

Tensile stretching parameters. For axial stretching a simple harmonic spring is used to determine the energy between all pairs of particles in the system (figure 3(*b*)), given by

$$\phi_{\text{T}}(\Delta r) = \tfrac{1}{2}k_{\text{T}}(r - r_0)^2 = \tfrac{1}{2}k_{\text{T}}\Delta r^2 \tag{9}$$

with k_{T} the spring constant relating distance, r, between two particles relative to the equilibrium distance, $r_0 = 25$ Å. Using the equivalent elastic strain energy,

$$U(\varepsilon) = \frac{1}{2}\int \sigma\varepsilon \,\mathrm{d}\Omega = \frac{1}{2}\frac{A_{\text{c}}E\Delta r^2}{r_0} = U(\Delta r). \tag{10}$$

Letting $\phi_{\text{T}}(\Delta r) = U(\Delta r)$,

$$k_{\text{T}} = \frac{A_{\text{c}}E}{r_0}. \tag{11}$$

For the mesoscale model, we do not consider a difference in armchair or zigzag orientation, and take $E = 0.968$ TPa. For the implemented square lattice, the cross-sectional area is taken as $A_{\text{c}} = r_0 t$, where r_0 is the equilibrium particle spacing and t is the sheet

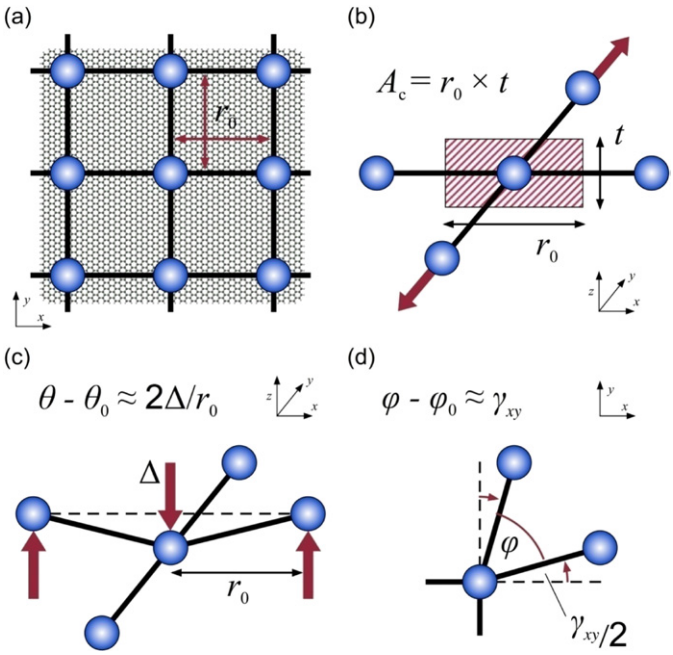

Figure 3. Schematic of the coarse-grain graphene model and derived mechanical potentials. (*a*) Square lattice model; each coarse-grain particle representative of 25 Å × 25 Å planar section of graphene sheet. (*b*) Geometric parameters for tensile stretching (bond) potential; associated cross-sectional area (A_c) equal to particle spacing (r_0) by sheet thickness (t). (*c*) Geometric parameters for out-of-plane bending (one-way); change in angle between defined particle triples, θ–θ_0, approximated by three-point bending. Each particle associated with two bending potentials (x- and y-direction). (*d*) Geometric parameters for in-plane distortion (shear); deviation from normal (90°) configuration, $\varphi - \varphi_0$, equal to shear strain, γ_{xy}. Each particle is associated with four shear potentials.

thickness. Thus, equation (11) reduces to $k_T = Et$. For multilayer graphene ribbons, $t = m \cdot D_{vdW}$, where m is the number of graphene layers. For example, for a monolayer ribbon, $k_T = Et = E D_{vdW} \cong 465\,\text{kcal mol}^{-1}\,\text{Å}^{-2}$. It is noted that, due to the linear harmonic function, stress at ultimate strain is higher than the physical value. However, due to the qualitative analysis of the current investigation, a linear relation is deemed adequate. Nonlinear behavior can easily be introduced for future studies.

Shear deformation parameters. For shear deformation, the strain is equivalent to in-plane bending (figure 3(*d*)), represented by a harmonic rotational-spring function:

$$\phi_\varphi(\Delta\varphi) = \tfrac{1}{2}k_\varphi(\varphi - \varphi_0)^2 = \tfrac{1}{2}k_\varphi \Delta\varphi^2 \tag{12}$$

with k_φ as the spring constant relating bending angle, φ, between three particles relative to the equilibrium angle, $\varphi_0 = 90°$. Using the equivalent elastic strain energy,

$$U(\gamma) = \frac{1}{2}\int \tau\gamma \, \mathrm{d}\Omega = \frac{1}{2}G\Omega\gamma^2. \tag{13}$$

Noting that

$$\Delta\varphi = \varphi - \varphi_0 = \gamma,$$

and letting $\phi_\varphi(\Delta\varphi) = U(\gamma)$,

$$k_\varphi = \tfrac{1}{4} G\Omega, \tag{14}$$

where a factor of one-fourth is introduced as there is four 90° angle potentials per particle. The associated volume is $\Omega = r_0^2 t$, where again t is a function of layers.

Out-of-plane bending parameter. For bending, the energy is given by a sum over all triples in the system (figure 3(*b*)), given by

$$\phi_\theta(\Delta\theta) = \tfrac{1}{2} k_\theta(\theta - \theta_0)^2 = \tfrac{1}{2} k_\theta \Delta\theta^2 \tag{15}$$

with k_θ the spring constant relating bending angle, θ, between three particles relative to the equilibrium angle, $\theta_0 = 180°$. Assuming three-point bending conditions, with a deflection, Δ, the equivalent elastic energy [57] is taken as

$$U(\Delta) = \frac{48EI}{(2r_0)^3}\Delta^2. \tag{16}$$

For small deformation,

$$\theta - \theta_0 \approx 2\Delta/r_0,$$

and letting $\phi_\theta(\Delta\theta) = U(\Delta)$:

$$k_\theta = \frac{3EI}{r_0}. \tag{17a}$$

The mechanical characterization of bending stiffness resulted in the bending modulus per unit width, D. To obtain the equivalent stiffness, $EI = Dr_0$. Subsequently,

$$k_\theta = 3D. \tag{17b}$$

There is no adjustment for the multilayer graphene, as each case was explicitly characterized atomistically.

Nonbonding interactions. Weak interactions (van der Waals adhesion) are defined by a Lennard-Jones 12 : 6 function, given by

$$\phi_{\text{adhesion}}(r) = 4\varepsilon_{\text{LJ}}\left(\left[\frac{\sigma_{\text{LJ}}}{r}\right]^{12} - \left[\frac{\sigma_{\text{LJ}}}{r}\right]^{6}\right), \tag{18}$$

with σ_{LJ} being the distance parameter and ε_{LJ} describing the energy well depth at equilibrium, calculated by multiplying the surface energy, γ_{L}, by the equivalent surface represented by the mesoscale model, or r_0^2.

Thus, the mesoscopic model is defined by a total of eight parameters: k_{T}, r_0, k_φ, φ_0, k_θ, θ_0, σ_{LJ} and ε_{LJ}. The results from the above atomistic simulations are used to determine the eight parameters via equilibrium conditions (r_0, φ_0, θ_0, σ_{LJ}) and energy conservation (k_{T}, k_φ, k_θ, ε_{LJ}). All parameters are defined solely from atomistic results given in tables 1 and 2.

All coarse-grain simulations are implemented using a modified version of the modeling code LAMMPS [38]. The LAMMPS code was modified to enable the treatment of graphene failure using simple cut-off methods for bond and angle potentials. Simulations used an *NVT* ensemble [58] with a temperature of 300 K and an integration timestep of 1 fs. A small viscous damping force (using a viscous force constant of approximately 0.1 pN per m s^{-1}) is introduced dissipate fluctuations during equilibration.

Table 2. Summary of parameters of the mesoscale model.

	No. of graphene layers				
Parameter	1	2	4	8	Units
k_T	470	930	1860	3720	kcal mol^{-1} Å^{-2}
r_0	25	25	25	25	Å
k_φ	16 870	33 740	67 480	134 960	kcal mol^{-1} rad^{-2}
φ_0	90°	90°	90°	90°	—
k_θ	144.9	8970	82 731	933 087	kcal mol^{-1} rad^{-2}
θ_0	180°	180°	180°	180°	—
σ	2.98	5.96	11.92	23.84	Å
ε	473	473	473	473	kcal mol^{-1}

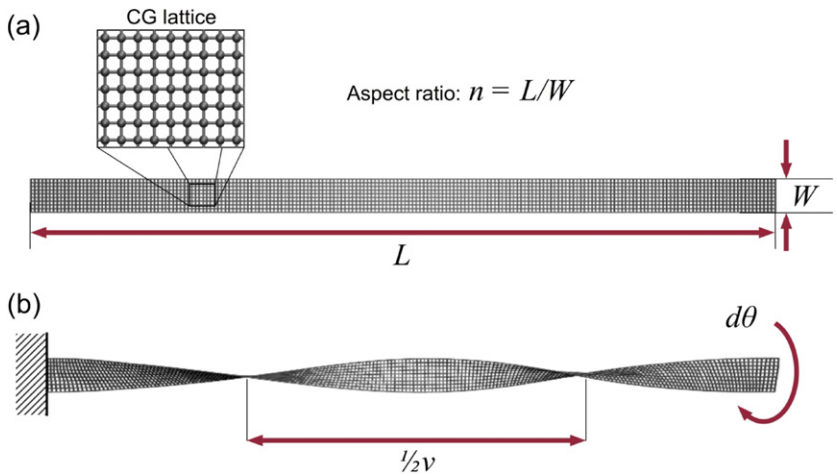

Figure 4. Schematic of graphene ribbon model. (*a*) Initial configuration: graphene ribbons defined by width (W), length (L) and aspect ratio (n). Aspect ratio at a constant $n = 20$, chosen to maintain stable, extended ribbon conformations [62]. The inset depicts the implemented coarse-grain lattice. (*b*) Twisted configuration: one end of graphene ribbon fixed, while the opposite end is subject to a twist angle, after which the ribbon is equilibrated and minimized with imposed periodicity (v).

2.3. Nanoribbon twist

The geometry of a rectangular graphene ribbon is defined by its width, W, and length, L ($L \gg W$), as shown in figure 4(*a*). The aspect ratio of the ribbon is defined as $n = L/W$. Physically, the edge shape (along the length) can be armchair or zigzag. Although the possible edge shape is critical to the electronic properties of graphene nanoribbons [59, 60], there is less effect on the mechanical behavior [61], and edge shape is not considered a variable in this study (all ribbons are considered to have armchair edges). All ribbons are initially constructed in a flat configuration, with a length of 500 nm and a width of either 25 nm ($n = 20$) or 50 nm ($n = 10$). It was previously shown that monolayer graphene maintains stable, extended ribbon-like structures for aspect ratios of this magnitude [62]. At approximately $n > 50$, entropic factors will dominate (and orientational order is kept only below this length-scale), and the ribbons tend to form wedges, loops or globular structures [62], hindering mechanical comparison.

To achieve a specific twist, MD simulations are undertaken in which the opposite free ends of the nanoribbon are held rigid. One end of the ribbon is fixed, while the opposite end is subject to an applied torsion moment for twist about the x-axis. A torsional strain rate of 720° per nanosecond (a rotational period of 0.5 ns) is applied. Using the geometric parameters L and $\mathrm{d}\theta$, we define the periodicity of the twisted ribbons, ν, as the minimum length of a ribbon to complete a full turn, that is, to cover a twist of 2π. We calculate the periodicity as

$$\nu = 2\pi.\frac{L}{\mathrm{d}\theta}. \tag{19}$$

The desired twist (or periodicity) determines the number of simulation timesteps using a constant torsional strain rate (that is, $\nu = 500$ nm requires 500 000 timesteps; $\nu = 1000$ nm requires only 250 000 timesteps, etc). After twisting is complete, the rotated end is subsequently fixed in the new, twisted configuration. The ribbon is then subject to equilibration at 300 K for 0.1 ns and minimization (conjugate-gradient algorithm implemented in the LAMMPS code). The periodicity is introduced as a variable to generalize structural conformations independently from the chosen ribbon length, L.

3. Results and discussion

Many of the exemplary characteristics of graphene depend on the geometrical structure of the 2D planar structure, and can thus be altered by geometric deformation. There have been full atomistic investigations characterizing potential graphene configurations [18, 62–64], but such studies have been limited in terms of accessible scale. The availability of the coarse-grained model allows us to reach significantly larger scales.

3.1. Variation in layers, twisted to helical ribbons

One of the advantages of implementing the current coarse-grain model is the ability to efficiently investigate multilayer (N-layer) graphene systems with the same computational effort. Here, a systematic comparison is made for 1-, 2-, 4- and 8-layer graphene systems. Whereas the tensile and shear stiffness terms are proportional to N, the out-of-plane bending stiffness is approximately proportional to N^3 (note that this does not hold for a single graphene sheet when $N = 1$) while the surface adhesion energy is constant for all models (see values in table 2). Imposed twist induces an initial curvature as well as a pre-stretch prior to characterization. As the twisted configurations have been dynamically attained and equilibrated (as opposed to the generation of ideal geometries), the effect of twist on their behavior is difficult to predict *a priori*.

Upon the initial applied end-rotation, all ribbons undertake periodic saddle-like chains (i.e. twisted ribbons), combined with a smooth increase in strain energy, indicating a constant configuration during the twist process (depicted in figure 5). For such a configuration, the edge graphene elements are subject to the most strain and curvature, while the center region is subject to the most twist [65]. It has been proposed that twisted ribbons could sustain significantly larger tensile strain due to intrinsic unwinding of the twisted structure subject to load [63]. However, for larger multilayer ribbons, there is significant pre-strain at the periphery of a twisted structure in excess of 10% (figure 6), limiting the ultimate tensile deformation. The concentrated strain is increased as the twist periodicity decreases, until the potential onset of ultimate strain and fracture (figure 5). For $W = 25$ nm, failure was incurred at a periodicity of ∼100 nm for the 8-layer model. This is indicative of a lower bound for the twisted ribbon configuration, as the peripheral strain is purely geometric and independent of model stiffness.

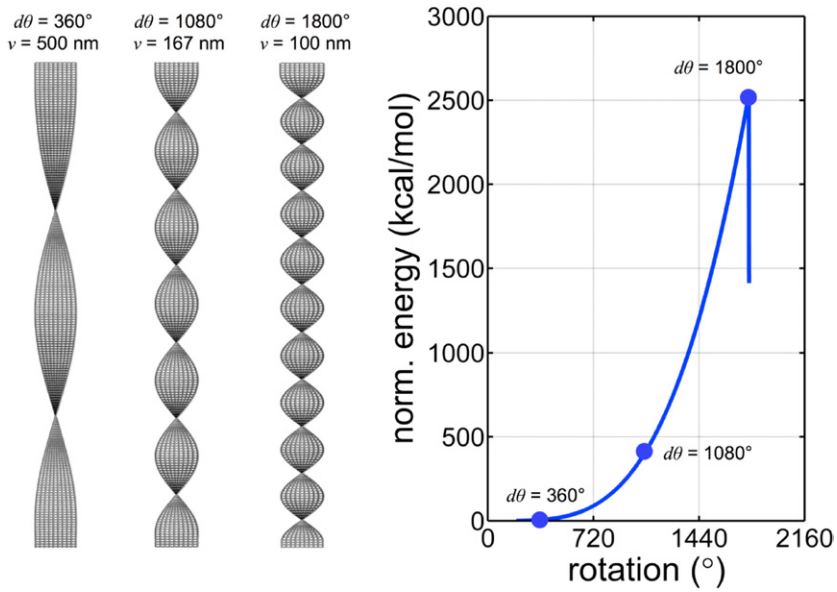

Figure 5. Simulation snapshots and strain energy evolution of a twisted eight-layer graphene ribbon. Strain energy normalized by $m \times n$, where m is the number of particles and n the number of represented layers. Due to the bending rigidity of the 8-layer model, the ribbon maintains a regular twisted configuration (saddle-like curvature) until ultimate failure due to tensile strain (at approximately 1800° of rotation or a periodicity of 100 nm).

However, the ribbons deviate from this configuration depending on the number of layers. For 1-, 2- and 4-layer models, there is a spontaneous transition into a 'helix' or coiled configuration—defined by a cylindrical wrapping—resulting in a more homogeneous strain field. A distinct transition in the strain energy evolution as a function of applied rotation occurs as the twisted ribbons subsequently collapse to a coil-like structure (figure 7). After undertaking a coil-like structure (figure 8), the strain energy gradient decreases, clearly indicating an energetically preferred ribbon configuration.

Experimental and computational studies have shown that the relationship between material properties and the macroscopic shape of chiral structures is surprisingly complex [65]. The transition from twisted to helical conformations has been investigated in other synthetic systems, attributed to the addition of chiral counterions [66], rearrangement of side-chains [67], temperature [68] and the interplay between molecular stiffness chirality [69]. Here, the system is subject to a mechanical force to artificially twist the ribbon from its equilibrium (i.e. flat/planar) configuration. Temperature fluctuations allow the system to explore conformational states. It has been shown that an increase in axial stiffness facilitates a coil-like structure [69]—here, increasing rotations have the same effect by increasing the tensile strain at the edges of the graphene, increasing the energy required to maintain a twisted, saddle-like state.

The observed structural transformation from twisted ribbons (saddle-like or Gaussian curvature) to helical ribbons (coil-like or cylindrical curvature) is associated with changes toward a more uniform and stable molecular configuration. Again, as depicted in figure 6, a decrease in periodicity induces large deviations in strain from the center to the edge of the ribbon. Additionally, across the ribbon, the relative twist is inhomogeneous—graphene sections at the periphery are less twisted than those near the center, whereas in the helical ribbon, the cylindrical curvature imposes similar twist throughout the width. Minimal strain energy

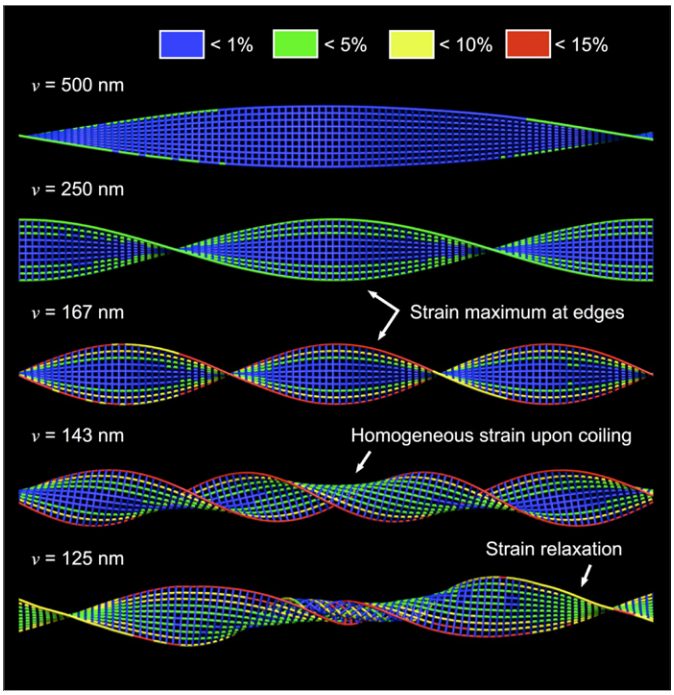

Figure 6. Simulation snapshots of twisted ribbon configuration depicting local strain. Images shown from 4-layer graphene ribbon, $n = 20$. Blue indicates strain less than 1%, green less than 5%, yellow less than 10% and red less than 15%. Strain distributions depict highest values and concentration toward the ribbon edges. As the periodicity decreases, the heterogeneity of the cross-sectional strain distribution increases. The collapse to a coil-like structure relaxes peripheral strains, and results in a more uniform, homogenous strain across the ribbon.

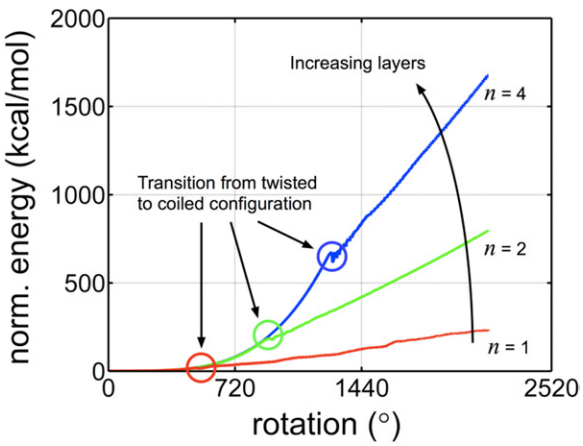

Figure 7. Normalized strain energy as a function of imposed rotation for 1-, 2- and 4-layer graphene models, $n = 20$. Smooth harmonic increase in strain energy as ribbons maintain regular twisted configuration. Abrupt transition to coiled configuration characterized by irregular strain energy, followed by a linear increase in strain energy at a lower rate. Transitions occur at periodicities of 337 nm, 191 nm and 141 nm for 1-, 2- and 4-layer models, respectively.

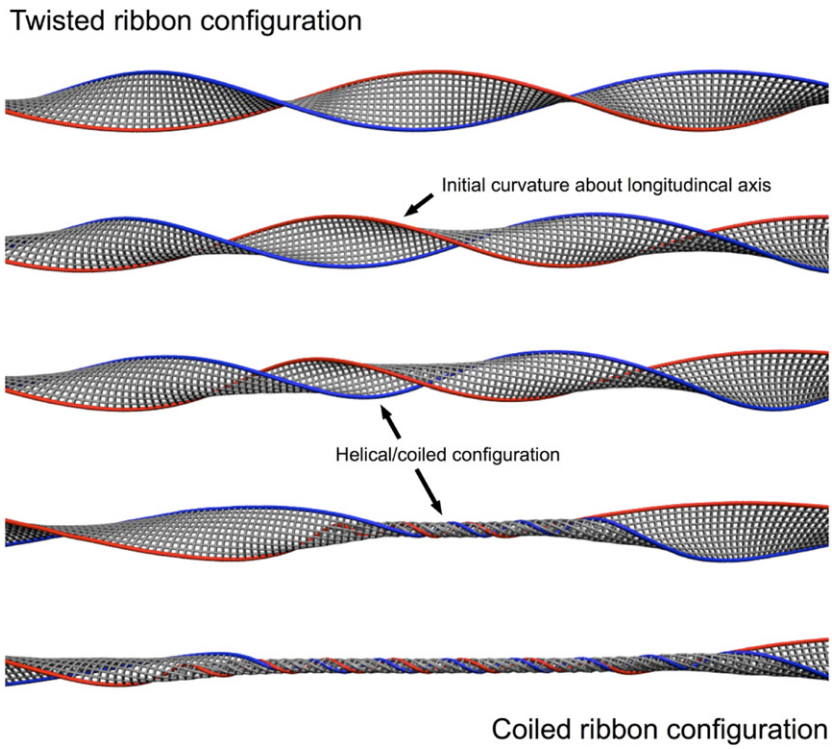

Figure 8. Simulation snapshots of twisted ribbon configuration to coiled ribbon configuration. Images shown from 2-layer graphene ribbon, $n = 20$. Opposite edges colored red and blue for clarity of conformational shape. Initial (top) snapshot at an imposed rotation of approximately 900°, where the ribbon maintains a regular, twisted ribbon structure. Collapse to coiled configuration occurs with minimal additional rotation (middle snapshots). The rotated ribbon preferentially undertakes a coiled configuration, which asserts more homogeneous strains and curvatures across the ribbon. Less strain energy is required in the coiled configuration to further increase $d\theta$ (see figure 7).

would favor the transformation of the kinetic twisted shape to the helical ribbon for a given imposed rotation. The consideration of the strain energy of the nanostructures suggests the transformation from twisted to helical ribbons results in a more uniform distribution of strain throughout the structure. Previous investigations have indicated a gradual crossover between Gaussian saddle-like curvature and cylindrical curvature as a function of the tensile stiffness—low stiffness resulting in twisted ribbons with higher stiffness resulting in helical ribbons with cylindrical curvature [69]. Imposed Gaussian curvature requires stretching the graphene, which is resisted by the tensile stiffness. As the applied twist is increased, greater curvature is energetically favorable to greater tensile strain. Thus, the collapse to a coiled configuration is due to an instability between the imposed strain of the twisted graphene ribbons and the bending stiffness (resisting curvature of coiled-configuration). It follows that stiffer ribbons should incur this transition at lower periodicities (in which the edge strain is increased), and thus multilayer graphene maintains a twisted configuration for shorter periodicities compared with monolayer graphene. Indeed, the transition periodicities for 1-, 2- and 4-layer models occur at 337 nm, 195 nm and 141 nm, respectively, as depicted in figure 7.

To further test this hypothesis, the width of the ribbons was increased to 50 nm ($n = 10$). This would have the dual effect of increasing the strain concentrations at the edges for a given

periodicity as well as decreasing the effective bending stiffness of the cross-section ($\sim W^{-1}$). For such ribbons, the twisted to coiled transition occurred at imposed periodicities of 623 nm, 416 nm and 344 nm for 1-, 2- and 4-layer models, respectively.

Predictive, analytical approaches for such transitions (i.e. the balance of curvature, chirality and adhesion energy) are limited to idealized structural configurations only [65], and do not explore the full range of potential shapes or mechanisms of shape transitions that even this simplified coarse-grain model depict. The obtained coiled ribbons are highly overlapped with non-constant curvatures and pitch, and do not undertake a perfect helical geometry (figure 7, for example). However, it is shown that the transition to coiled configurations is clearly dependent on the initial geometry of the graphene ribbon, which can be coerced to either twisted or coiled configurations.

3.2. Stability of coiled ribbons

Stable graphene structures can result via a balance of elastic energy and weak van der Waals interactions [31, 62, 70] developing an energetic minima. As the surface adhesion strength is constant regardless of the number of graphene layers, stability is dependent on the bending stiffness of the graphene model. It has been shown that multilayer systems require relatively low curvatures for stable self-folding [31]. Thus, we anticipate only stable coiled configurations for monolayer graphene ribbons, which have relatively high imposed curvature.

During the twisting, we compute the adhesion energy along with the strain energy, where the components of equation (8) are separated:

$$\phi_{\text{system}} = [\phi_{\text{T}} + \phi_{\varphi} + \phi_{\theta}] + \phi_{\text{adhesion}} = \phi_{\text{strain}} + \phi_{\text{adhesion}}. \tag{20}$$

Plotting the total, strain and adhesion energies as a function of imposed rotation for monolayer graphene with $n = 20$ (figure 9), we clearly see (1) the transition to a coil-like structure is indicated by a decrease in adhesion energy (intersheet adhesion is preferential) and (2) a local minimum at a rotation of approximately 1025° ($v = 176$ nm). This energetic minimum suggests a stable structure. To determine structural stability, the ribbon was subject to a rotation of 1080°, followed by removal of the end constraints. The structure is then equilibrated for 1 ns at 300 K, maintaining the coiled configuration.

An increase in ribbon width serves to increase the available surface area for adhesion, as well as decrease the effective cross-sectional bending stiffness and required curvature for coiled states. Thus, a stable coiled structure was anticipated for monolayer graphene with an aspect ratio decreased to $n = 10$. Plotting the total, strain and adhesion energies as a function of imposed rotation (figure 10) indicates a stable configuration at both 759° and 1782°. The first stable coiled configuration occurs at an imposed rotation less than the previous case (1025° with $n = 20$) as expected. The second stable configuration occurs as the coiled ribbon collapses onto itself in a tighter cylindrical arrangement—resulting in the adhesion energy contribution to decreases at a greater rate than the strain energy required to impose rotation. Both configurations were unconstrained and equilibrated for 1.0 ns at 300 K to ensure stability.

In addition, full atomistic investigations indicate covalent bond formation between carbon atoms of twisted graphene ribbons [63]. Although not reflected by the coarse-grain model, such covalent bond formation would further stabilize the coiled structure. The appearance of such stable configurations suggests that twisted graphene nanoribbons can be manipulated into various nanostructures, potentially allowing high-surface accessible areas, controlled coils, etc, that can have great impact on the associated mechanical and electrical properties.

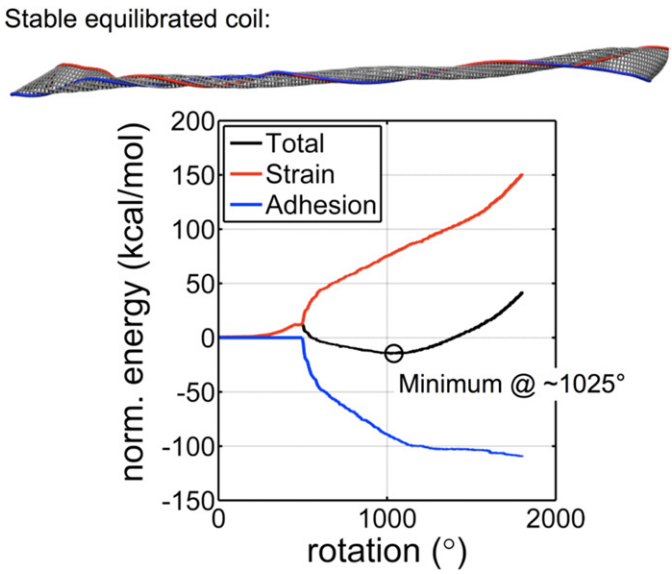

Figure 9. Stable configuration of monolayer graphene, $n = 20$: schematic of equilibrated coil, after an applied rotation and release of the end constraints, graphene ribbon maintains convoluted structure (top). Plot of total, strain and adhesion energies as a function of imposed rotation. The transition to a coil-like structure is clearly indicated by a decrease in adhesion energy (intersheet adhesion is preferential). Further, a local minimum is indicated rotation of approximately 1025° ($v = 176$ nm), suggesting a stable, coiled configuration.

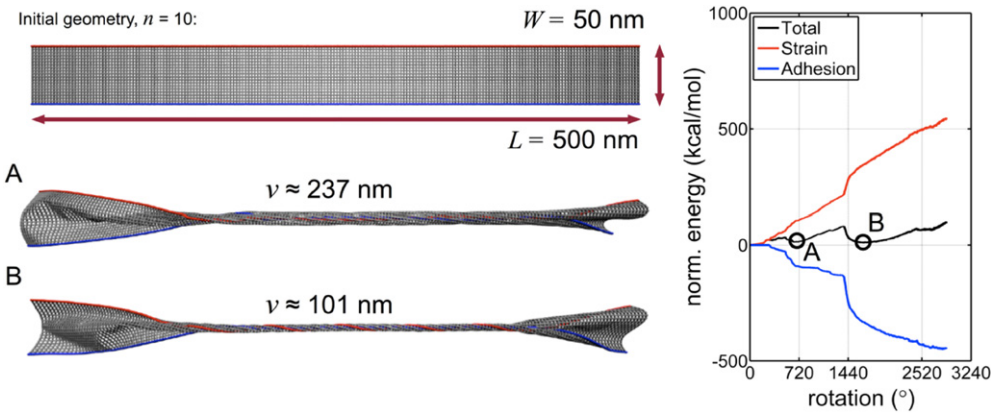

Figure 10. Stable configurations of monolayer graphene, $n = 10$: Schematics of initial structure of graphene ribbon, $n = 10$, as well as equilibrated coil structures (A and B), after an applied rotation of 765° and 1800°, respectively (left). Plot of total, strain and adhesion energies as a function of imposed rotation (right). Again, the transition to a coil-like structure is clearly indicated by a decrease in adhesion energy. Local minima occurs at rotations of approximately 759° ($v = 237$ nm) and 1782° ($v = 101$ nm).

4. Conclusion

The nanostructural geometry of graphene sheets and ribbons is critical for their unique properties and holds the potential for large-scale electronics and device applications.

With coarse-grained models, more complex structures may be investigated, allowing the development of new graphene-based composites [5], or graphene materials with unique electrical [6–8, 16] or thermal [71] properties. The mesoscale model described herein allows a new approach for the investigation of graphene nanostructures on the order of micrometers and at very long time-scales. Probing the potential shapes and associated mechanical properties of graphene ribbons, we have shown that the ribbon shape—twisted or coiled—can manipulated by adjusting the imposed rotation. The predictions put forth based on our simulations provide a challenge to experimentalists to explore this aspect. Precise control of the twisted ribbons can lead to the design new structures for nanotechnology, exploiting both the intrinsic properties of graphene with predictable geometric configurations.

Further, the coarse-graining approach presented here can be extended to other materials such as polymer nanofilms [22, 23], cell membranes [24], plant cell structures [72], or other two-dimensional systems [73], providing an efficient means to implement material models at the nano- and microscales to facilitate the development of new nanomaterials and devices. The effect of a twisted structure coupled with its mechanical properties finds application beyond synthetic graphene systems, as a twisted geometric configuration is a universal feature of many biological structures such as tropocollagen or alpha-helices [74, 75], DNA 76, as well as amyloid fibrils [77].

Acknowledgments

This work was supported primarily by the MRSEC Program of the National Science Foundation under award number DMR-0819762, with additional support provided by DOD-MURI. The calculations and the analysis were carried out using a parallelized LINUX cluster at MIT's Laboratory for Atomistic and Molecular Mechanics (LAMM). Visualization has been carried out using the VMD visualization package [78].

References

[1] Duplock E J, Scheffler M and Lindan P J D 2004 Hallmark of perfect graphene *Phys. Rev. Lett.* **92** 225502
[2] Ohta T *et al* 2006 Controlling the electronic structure of bilayer graphene *Science* **313** 951–4
[3] Lee C *et al* 2008 Measurement of the elastic properties and intrinsic strength of monolayer graphene *Science* **321** 385–8
[4] Zhao Q Z, Nardelli M B and Bernholc J 2002 Ultimate strength of carbon nanotubes: a theoretical study *Phys. Rev.* B **65** 144105
[5] Stankovich S *et al* 2006 Graphene-based composite materials *Nature* **442** 282–6
[6] Liu C G *et al* 2010 Graphene-based supercapacitor with an ultrahigh energy density *Nano Lett.* **10** 4863–8
[7] Stoller M D *et al* 2008 Graphene-based ultracapacitors *Nano Lett.* **8** 3498–502
[8] Rogers J A, Someya T and Huang Y G 2010 Materials and mechanics for stretchable electronics *Science* **327** 1603–7
[9] Meyer J C *et al* 2007 On the roughness of single- and bi-layer graphene membranes *Solid State Commun.* **143** 101–9
[10] Ci L *et al* 2008 Controlled nanocutting of graphene *Nano Res.* **1** 116–22
[11] Sen D *et al* 2010 Tearing graphene sheets from adhesive substrates produces tapered nanoribbons *Small* **6** 1108–16
[12] Li X L *et al* 2008 Chemically derived, ultrasmooth graphene nanoribbon semiconductors *Science* **319** 1229–32
[13] Meyer J C *et al* 2007 The structure of suspended graphene sheets *Nature* **446** 60–3
[14] Li Q *et al* 2009 Real-time study of graphene's phase transition in polymer matrices *Nano Lett.* **9** 2129–32
[15] Fasolino A, Los J H and Katsnelson M I 2007 Intrinsic ripples in graphene *Nature Mater.* **6** 858–61
[16] Xu Z P and Buehler M J 2009 Hierarchical graphene nanoribbon assemblies feature unique electronic and mechanical properties *Nanotechnology* **20** 375704

[17] Katsnelson M I and Geim A K 2008 Electron scattering on microscopic corrugations in graphene *Phil. Trans. R. Soc.* A **366** 195–204
[18] Shenoy V B *et al* 2008 Edge-stress-induced warping of graphene sheets and nanoribbons *Phys. Rev. Lett.* **101** 245501
[19] Scarpa F, Adhikari S and Srikantha Phani A 2009 Effective elastic mechanical properties of single layer graphene sheets *Nanotechnology* **20** 065709
[20] Tserpes K I and Papanikos P 2005 Finite element modeling of single-walled carbon nanotubes *Compos. B: Eng.* **36** 468–77
[21] Meo M and Rossi M 2006 Prediction of Young's modulus of single wall carbon nanotuves by molecular-mechancis based finite element modelling *Compos. Sci. Technol.* **66** 1597–605
[22] Dai X H *et al* 2005 Mechanical properties of polyelectrolyte multilayer self-assembled films *Thin Solid Films* **474** 159–64
[23] Thompson M T *et al* 2005 Tuning compliance of nanoscale polyelectrolyte multilayers to modulate cell adhesion *Biomaterials* **26** 6836–45
[24] Arslan M *et al* 2008 Constitutive modeling of the stress-stretch behavior of two-dimensional triangulated macromolecular networks containing folded domains *J. Appl. Mech.—Trans. ASME* **75** 011020
[25] Cranford S W and Buehler M J 2010 In silico assembly and nanomechanical characterization of carbon nanotube buckypaper *Nanotechnology* **21** 265706
[26] Cranford S and Buehler M J 2009 Mechanomutable carbon nanotube arrays *Int. J. Mater. Struct. Integrity* **3** 161–78
[27] Bratzel G H *et al* 2010 Bioinspired noncovalently crosslinked 'fuzzy' carbon nanotube bundles with superior toughness and strength *J. Mater. Chem.* **20** 10465–74
[28] Buehler M J 2006 Mesoscale modeling of mechanics of carbon nanotubes: Self-assembly, self-folding and fracture *J. Mater. Res.* **21** 2855–69
[29] Buehler M J 2006 Atomistic and continuum modeling of mechanical properties of collagen: elasticity, fracture, and self-assembly *J. Mater. Res.* **21** 1947–61
[30] Buehler M J 2008 Nanomechanics of collagen fibrils under varying cross-link densities: atomistic and continuum studies *J. Mech. Behav. Biomed. Mater.* **1** 59–67
[31] Cranford S, Sen D and Buehler M J 2009 Meso-origami: folding multilayer graphene sheets *Appl. Phys. Lett.* **95** 123121
[32] Strachan A *et al* 2005 Thermal decomposition of RDX from reactive molecular dynamics *J. Chem. Phys.* **122** 054502
[33] Chenoweth K, van Duin A C T and Goddard W A 2008 ReaxFF reactive force field for molecular dynamics simulations of hydrocarbon oxidation *J. Phys. Chem.* A **112** 1040–53
[34] van Duin A C T *et al* 2001 ReaxFF: a reactive force field for hydrocarbons *J. Phys. Chem.* A **105** 9396–409
[35] Nielson K D *et al* 2005 Development of the ReaxFF reactive force field for describing transition metal catalyzed reactions, with application to the initial stages of the catalytic formation of carbon nanotubes *J. Phys. Chem.* A **109** 493–9
[36] Chen N *et al* 2005 Mechanical properties of connected carbon nanorings via molecular dynamics simulation *Phys. Rev.* B **72** 085416
[37] Berendsen H J C *et al* 1984 Molecular-dynamics with coupling to an external bath *J. Chem. Phys.* **81** 3684–90
[38] Plimpton S J 1995 Fast parallel algorithms for short-range molecular dynamics *J. Comput. Phys.* **117** 1–19
[39] Robertson D H, Brenner D W and Mintmire J W 1992 Energetics of nanoscale graphite tubules *Phys. Rev.* B **45** 12592–5
[40] Tomanck D, Zhong W and Krastev E 1993 Stability of multishell fullerenes *Phys. Rev.* B **48** 15461–4
[41] Ruoff R S, Qian D and Liu W K 2003 Mechanical properties of carbon nanotubes: theoretical predictions and experimental measurements *C.R. Physique* **4** 993–1008
[42] Wei X D *et al* 2009 Nonlinear elastic behavior of graphene: ab initio calculations to continuum description *Phys. Rev.* B **80** 205407
[43] Lu Q and Huang R 2009 Nonlinear mechanics of single-atomic-layer graphene sheets *Int. J. Appl. Mech.* **1** 443–67
[44] Zhou J and Huang R 2008 Internal lattice relaxation of single-layer graphene under in-plane deformation *J. Mech. Phys. Solids* **56** 1609–23
[45] Tsai D H 1979 The virial theorem and stress calculation in molecular dynamics *J. Chem. Phys.* **70** 1375–82
[46] Zimmerman J A *et al* 2004 Calculation of stress in atomistic simulation *Modelling Simul. Mater. Sci. Eng.* **12** S319–32
[47] Sakhaee-Pour A 2009 Elastic properties of single-layered graphene sheet *Solid State Commun.* **149** 91–5

[48] Kudin K N, Scuseria G E and Yakobson B I 2001 C2F, BN, and C nanoshell elasticity from ab initio computations *Phys. Rev.* B **64** 235406
[49] Arroyo M and Belytschko T 2004 Finite crystal elasticity of carbon nanotubes based on the exponential Cauchy–Born rule *Phys. Rev.* B **69** 115415
[50] Liu F, Ming P M and Li J 2007 Ab initio calculation of ideal strength and phonon instability of graphene under tension *Phys. Rev.* B **76** 064120
[51] Huang Y, Wu J and Hwang K C 2006 Thickness of graphene and single-wall carbon nanotubes *Phys. Rev.* B **74** 245413
[52] Grantab R, Shenoy V B and Ruoff R S 2010 Anomalous strength characteristics of tilt grain boundaries in graphene *Science* **330** 946–8
[53] Lu Q, Arroyo M and Huang R 2009 Elastic bending modulus of monolayer graphene *J. Phys. D: Appl. Phys.* **42** 102002
[54] Landau L D *et al* 1986 *Theory of Elasticity* (*Course of Theoretical Physics*) 3rd English edn, vol 7 (Oxford/New York: Pergamon) 187pp
[55] Zong Z *et al* 2010 Direct measurement of graphene adhesion on silicon surface by intercalation of nanoparticles *J. Appl. Phys.* **107** 026104
[56] Henry D J *et al* 2005 Adhesion between graphite and modified polyester surfaces: a theoretical study *J. Phys. Chem.* B **109** 17224–31
[57] Timoshenko S and Maccullough G H 1940 *Elements of Strength of Materials* 2nd edn (New York: D Van Nostrand Company, Inc.)
[58] Hoover W G 1985 Canonical dynamics—equilibrium phase-space distributions *Phys. Rev.* A **31** 1695–7
[59] Xu Z P, Zheng Q S and Chen G H 2007 Elementary building blocks of graphene-nanoribbon-based electronic devices *Appl. Phys. Lett.* **90** 223115
[60] Son Y W, Cohen M L and Louie S G 2006 Energy gaps in graphene nanoribbons *Phys. Rev. Lett.* **97** 216803
[61] Xu Z P 2009 Graphene nano-ribbons under tension *J. Comput. Theor. Nanosci.* **6** 625–8
[62] Xu Z P and Buehler M J 2010 Geometry controls conformation of graphene sheets: membranes, ribbons, and scrolls *ACS Nano* **4** 3869–76
[63] Li Y 2010 Twist-enhanced stretchability of graphene nanoribbons: a molecular dynamics study *J. Phys. D: Appl. Phys.* **43** 495405
[64] Bets K V and Yakobson B I 2009 Spontaneous twist and intrinsic instabilities of pristine graphene nanoribbons *Nano Res.* **2** 161–6
[65] Selinger J V, Spector M S and Schnur J M 2001 Theory of self-assembled tubules and helical ribbons *J. Phys. Chem.* B **105** 7157–69
[66] Oda R *et al* 1999 Tuning bilayer twist using chiral counterions *Nature* **399** 566–9
[67] Pashuck E T and Stupp S I 2010 Direct observation of morphological tranformation from twisted ribbons into helical ribbons *J. Am. Chem. Soc.* **132** 8819–21
[68] Spector M S *et al* 2001 Chiral self-assembly of nanotubules and ribbons from phospholipid mixtures *Nano Lett.* **1** 375–8
[69] Selinger R L B *et al* 2004 Shape selection in chiral self-assembly *Phys. Rev. Lett.* **93** 158103
[70] Shi X H, Pugno N M and Gao H J 2010 Tunable core size of carbon nanoscrolls *J. Comput. Theor. Nanosci.* **7** 517–21
[71] Balandin A A *et al* 2008 Superior thermal conductivity of single-layer graphene *Nano Lett.* **8** 902–7
[72] Ghysels P *et al* 2009 Multi-scale simulation of plant tissue deformation using a model for individual cell mechanics *Phys. Biol.* **6** 016009
[73] Zhang H T and Sun C T 2006 A multiscale mechanics approach for modeling textured polycrystalline thin films with nanothickness *Int. J. Mech. Sci.* **48** 899–906
[74] Bozec L, van der Heijden G and Horton M 2007 Collagen fibrils: nanoscale ropes *Biophys. J.* **92** 70–5
[75] Uzel S G M and Buehler M J 2009 Nanomechanical sequencing of collagen: tropocollagen features heterogeneous elastic properties at the nanoscale *Integrative Biol.* **1** 452–9
[76] Gore J *et al* 2006 DNA overwinds when stretched *Nature* **442** 836–9
[77] Paparcone R and Buehler M J 2009 Microscale structural model of Alzheimer A β(1-40) amyloid fibril *Appl. Phys. Lett.* **94** 243904
[78] Humphrey W, Dalke A and Schulten K 1996 VMD: Visual molecular dynamics *J. Mol. Graph.* **14** (1) 33–8